

pubs.acs.org/est Article

# Tailoring Thermoresponsive Polymer Architecture to Enhance Antifouling and Fouling Reversibility of Membranes

Inhyeong Jeon,<sup>#</sup> Junwoo Lee,<sup>#</sup> Mingjiang Zhong,\* and Jae-Hong Kim\*



Cite This: Environ. Sci. Technol. 2023, 57, 17610-17619



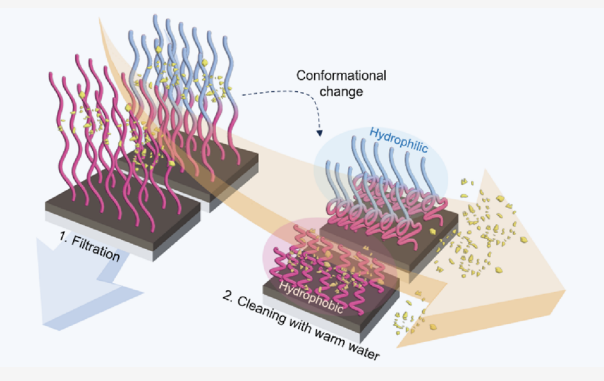
**ACCESS** 

III Metrics & More

Article Recommendations

si Supporting Information

ABSTRACT: Cleaning a fouled membrane using warm water, instead of commonly used fouling control chemicals, is an approach advocated in resource-limited settings, where small-scale membrane filtration is used to provide clean water. Thermoresponsive polymers coated onto membranes undergo a conformational change across their lower critical solution temperature (LCST), enabling foulant removal during such temperature-swing cleaning. However, their intrinsic hydrophobicity above the LCST poses a fundamental material challenge. In this study, we examine how thermoresponsive polymers can be optimally copolymerized with hydrophilic polymers by precisely manipulating monomer arrangement of thermoresponsive *N*-isopropylacry-lamide and hydrophilic 2-[2-(2-methoxyethoxy)ethoxy]ethyl



acrylate. We successfully grafted these copolymers with different monomer arrangements onto poly(ether sulfone) ultrafiltration membranes while maintaining other polymer characteristics, such as the degree of polymerization and grafting density, constant. We found that placing hydrophilic polymer blocks at the outermost surface above the thermoresponsive polymer blocks is critical to achieving high surface hydrophilicity while preserving the thermoresponsive functionality. We demonstrate enhanced fouling resistance and efficient temperature-swing cleaning with optimized copolymer design based on their interaction with bovine serum albumin during static adsorption, filtration, and cleaning processes. These findings emphasize the importance of accurately tailoring the polymer architecture to enable more efficient filtration with reduced fouling and the capability to effectively clean the fouled membrane by simply using warm water.

KEYWORDS: membrane fouling, thermoresponsive polymer, lower critical solution temperature (LCST), antifouling, fouling reversibility

### **■** INTRODUCTION

Millions of people in rural areas of low- to medium-income countries (LMICs) still lack access to basic drinking water services, 1-3 despite recent technological advances in water treatment. In LMICs, ultrafiltration has been widely considered a viable small-scale water supply method because of its demonstrated efficacy in removing pathogens such as bacteria and viruses, as well as its cost-effectiveness and ease of operation.<sup>4,5</sup> Nevertheless, membrane fouling remains a substantial technical challenge, 6,7 diminishing membrane performance and lifespan and ultimately increasing costs associated with cleaning and operation.<sup>8,9</sup> Surface modification with various coating agents such as hydrophilic polymers has been widely explored to enhance antifouling properties.<sup>10</sup> However, prolonged use inevitably leads to membrane blockage, rendering most surface modification strategies ineffective. Membrane fouling presents additional difficulties in rural areas of LMICs where conventional membrane cleaning methods using chemicals such as oxidants and strong acids are often impractical. One promising solution involves the modification of the membrane surface via grafting

thermoresponsive polymers. <sup>11,12</sup> The rapid conformational change that occurs across the lower critical solution temperature (LCST) serves as the basis for the idea of temperature-swing cleaning; *i.e.*, to disturb the fouling layer and wash off the foulants <sup>13–15</sup> simply by using warm water, which is readily available in most settings.

One of the most studied thermoresponsive polymers is poly(N-isopropylacrylamide) (PNIPAM).  $^{16,17}$  Below its LCST of approximately 32 °C, PNIPAM exhibits hydrophilic properties with a stretched conformation due to hydrogen bonding between amide groups in PNIPAM chains and water molecules.  $^{14}$  Some studies have grafted PNIPAM onto membranes with the sole goal of enhancing hydrophilicity and antifouling properties.  $^{11-15,18,19}$  However, above the

Received: July 12, 2023 Revised: October 17, 2023 Accepted: October 18, 2023 Published: November 1, 2023





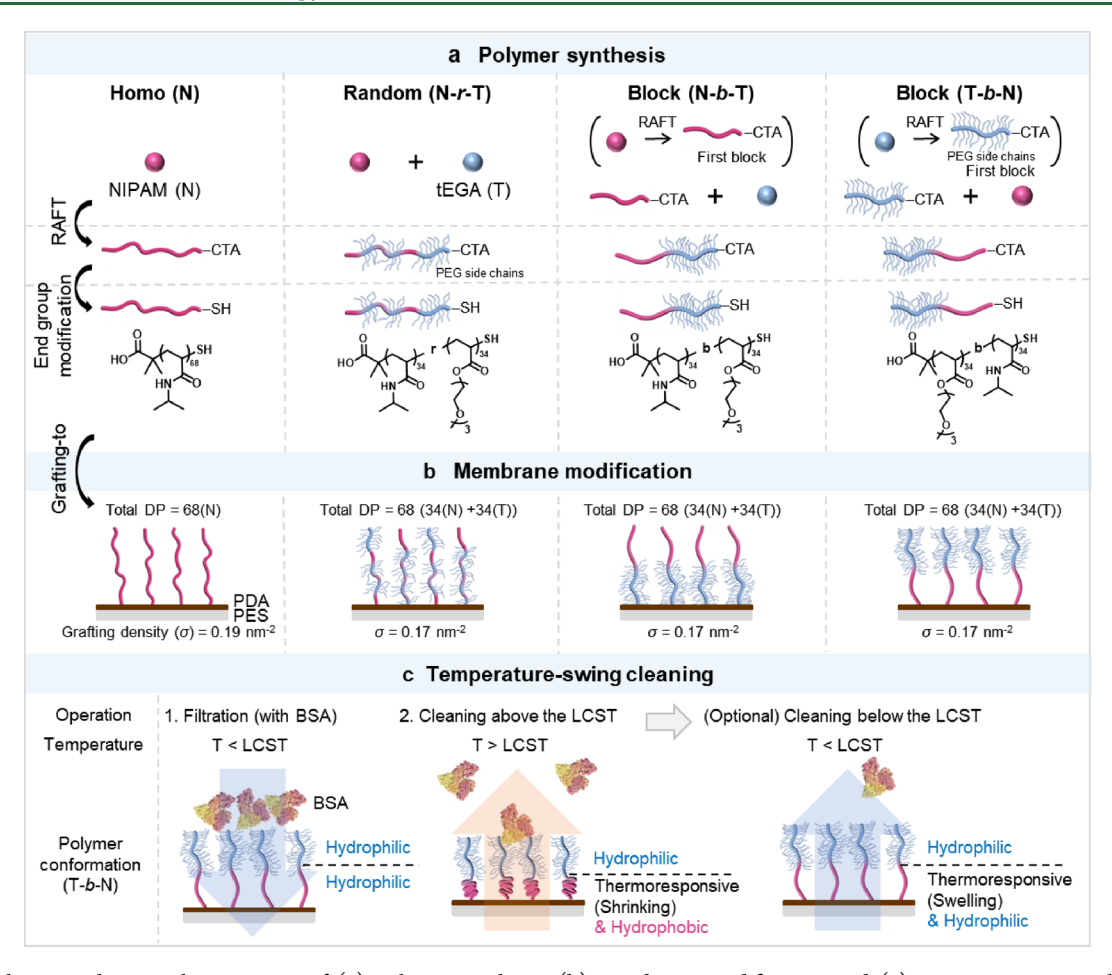


Figure 1. Schematic showing the processes of (a) polymer synthesis, (b) membrane modification, and (c) temperature swing-cleaning. Two cleaning methods were investigated in this study; (1) backwashing at a temperature above the LCST and (2) backwashing at a temperature above the LCST followed by backwashing at a temperature below the LCST (alternate temperature change cleaning).

LCST, PNIPAM chains undergo a transition to a hydrophobic state, resulting in a rapid collapse into a globular conformation due to increased hydrophobic interactions and disrupted hydrogen bonding. Although this hydrophilic-to-hydrophobic transition is essential for conformational change and disruption of the fouling layer, the PNIPAM-based cleaning strategy encounters a conceptual limitation due to PNIPAM's hydrophobic nature above the LCST, which hinders the desorption of foulants.

Incorporating an additional hydrophilic polymer into PNIPAM while maintaining its thermoresponsive nature presents a logical solution to this challenge. Various studies have investigated the introduction of hydrophilic poly(ethylene glycol) (PEG) derivative side chains into PNIPAM in order to enhance the hydrophilicity of the resulting copolymer and improve the surface cleaning performance. However, conflicting results have been reported, with some studies demonstrating improved performance while others claiming that hydrophilic copolymers are ineffective. <sup>13,20–22</sup> We find a quantitative comparison of past reports difficult due to insufficient information regarding the synthesized polymer and uncontrolled structural parameters. Factors such as the degree of polymerization (DP) and grafting density play a crucial role in influencing the conformational changes around the LCST. 23,24 The unprecise control over these parameters can result in variations in the copolymer's behavior and, consequently, its effectiveness in addressing fouling. Unfortunately, many

studies utilizing PNIPAM for membrane modification often lack essential material characterization information. In addition, there are considerable inconsistencies in the reported DP and grafting densities among different studies.

In this work, we seek to elucidate the specific influence of monomer arrangements in grafted thermoresponsive copolymers on the antifouling properties and fouling reversibility. We synthesized four different types of linear polymers (i.e., homopolymer, random copolymer, and two block copolymers) with the same total DP of 68 using NIPAM and hydrophilic 2-[2-(2-methoxyethoxy)ethoxy]ethyl acrylate (tEGA) via reversible addition—fragmentation chain transfer (RAFT) polymerization. After end-group modification to thiol, these thiolterminated polymers were attached onto the polydopaminecoated poly(ether sulfone) (PES) ultrafiltration membranes by a Michael addition reaction.<sup>25</sup> Here, we used the "grafting-to" technique, which involves synthesizing the polymer separately and then covalently attaching it to the membrane surface.<sup>26</sup> This approach enables precise characterization of the attached polymer, unlike the alternative "grafting-from" technique, 27 and ensures homogeneous coverage of the substrate surface with dense polymer brushes.<sup>28</sup> Given the proven efficacy of antifouling properties for substrates grafted by the polymers with DPs between 50 and 100,<sup>26</sup> we settled on the DP of 68 for our study. We examined the physicochemical properties and separation performance of the pristine and modified membranes and conducted static and dynamic fouling

experiments using bovine serum albumin (BSA). By meticulously controlling the DP and grafting density, this study presents, for the first time, critical insights into how monomer arrangements and block sequences influence the antifouling properties and fouling reversibility of the membranes during temperature-swing cleaning.

## EXPERIMENTAL SECTION

**Materials and Chemicals.** NIPAM (99%), 2-(dodecylthiocarbonothioylthio)-2-methylpropionic acid (DDMAT, 98%), azobis(2-methylpropionitrile) (AIBN, 98%), 1,4-dioxane (anhydrous, 99.8%), *N,N*-dimethylformamide (DMF, anhydrous, 99.8%), diethyl ether (HPLC grade), hexanes (98.5%), tetrahydrofuran (THF, HPLC grade), and butylamine (99.5%) were purchased from Sigma-Aldrich (St. Louis, MO). tEGA was purchased from TCI America (Portland, OR), PES membranes from Pall Corporation (New York, NY), 2-amino-2-(hydroxymethyl)-1,3-propanediol hydrochloride (TRIS·HCl, 98%) from TCI, and dopamine hydrochloride, BSA (98%), sodium dodecyl sulfate (SDS, 99%), PEGs and phosphate buffered saline (PBS) from Sigma-Aldrich. Deionized water (DI, > 18.2 MΩ cm) from a Milli-Q system was used to prepare experimental solutions.

Synthesis of Polymers. We employed the RAFT polymerization technique to obtain target thermoresponsive polymers with a precisely controlled number-average molecular weight  $(M_n)$  with low dispersity (D), <sup>29</sup> as shown in Figure 1a. The homopolymer PNIPAM<sub>68</sub> terminated with trithiocarbonate (PNIPAM<sub>68</sub>-CTA, Figure S1) was synthesized by using DDMAT as the chain transfer agent (CTA) and AIBN as an initiator in 1,4-dioxane with a [NIPAM]:[DDMAT]:[AIBN] ratio of 100:1:0.1. After the mixture was stirred for 50 min at 70 °C under a nitrogen atmosphere, the polymer was precipitated from diethyl ether and the precipitates were dried under a vacuum at room temperature for 12 h. The chemical structure and DP were determined via <sup>1</sup>H-nuclear magnetic resonance (NMR) spectroscopy using a 500 MHz Agilent DD2 NMR spectrometer with deuterated dimethyl sulfoxide (DMSO-d<sub>6</sub>) as a solvent (<sup>1</sup>H NMR (500 MHz, DMSO- $d_6$ ,  $\delta$ ): 7.23–6.46 (br, – NH), 3.94–3.79 (br, – CH), 2.17-1.86 (br, -CH), 1.75-1.20 (br,  $-CH_2$ ), 1.14-0.99 (br,  $-CH_3$ ), 0.89–0.81 (br,  $-CH_3$ ), Figure S2). The experimental procedures for synthesizing the random copolymer and two block copolymers with trithiocarbonate group (i.e., P-(NIPAM<sub>34</sub>-r-tEGA<sub>34</sub>)-CTA, P(NIPAM<sub>34</sub>-b-tEGA<sub>34</sub>)-CTA, and P(tEGA<sub>34</sub>-b-NIPAM<sub>34</sub>)-CTA) followed overall similar procedures and details are summarized in Texts S1 - S3 and Figures S1 - S2. The procedure for the polymerization kinetics experiment is described in Text S4, the  $M_n$  and D were determined using the gel permeation chromatography (GPC) with DMF as an eluent with the calibration of polystyrene standard. The monomer conversion ratio of PNIPAM and PtEGA as a function of reaction time is shown in Figure S3.

Small-Angle X-ray Scattering (SAXS) Measurement. All materials were annealed under a vacuum at 110 °C for 1 h before SAXS measurement. The vacuum oven was allowed to cool to ambient temperature and then vented to the atmosphere. The SAXS measurement was conducted using Xenocs Xeuss 3.0 equipped with a microfocus sealed-tube Cu 30 W/30  $\mu$ m X-ray source (Cu K- $\alpha$ ,  $\lambda$  = 1.54 Å).

**LCST Measurement.** The LCST of the polymer–CTA was determined by monitoring turbidity change in water suspension (0.5 wt %) using UV–vis spectroscopy (UV–vis

Shimadzu UV-3600Plus) equipped with a temperature controller. The mixture was placed in a sample cell, heated at a rate of 1 °C per min from 25 to 75 °C, stayed at 75 °C for 5 min, and was cooled at the same rate of 1 °C per min from 75 to 25 °C. The LCST was defined as the average temperature where a fall in optical transmittance to 50% of the initial value was observed in heating and cooling curves. <sup>30,31</sup>

End Group Modification of Synthesized Polymers to Thiol Functional Group. The polymer-CTA (1 g) was redissolved in 10 mL of THF and butylamine was added to produce a thiol-terminated polymer (polymer-SH, Figure S1 and Figure 1a) via aminolysis.<sup>32</sup> The reaction was carried out in a nitrogen atmosphere at room temperature for 5 h, during which a noticeable color change from yellow to colorless was observed. The product was precipitated in hexane, and the white precipitates were dried under a vacuum at room temperature for 12 h. The chemical structure before and after the aminolysis was confirmed via <sup>1</sup>H NMR spectroscopy and attenuated total reflectance Fourier transform infrared spectroscopy (ATR-FTIR, IRTracer-100, Shimadzu). The absorption spectra of polymers were measured by UV-vis spectroscopy using a Varian Cary 50 Bio UV-visible spectrophotometer.

Pretreatment and Surface Modification of Membranes. The PES membrane coupons were soaked in ethanol for a few hours, rinsed with DI water, and dried under a vacuum at room temperature before use. The first step before attaching the polymers onto the membrane surface was depositing a polydopamine (PDA) layer on the membrane. 33,34 Briefly, the membrane coupon was placed onto a glass plate with its active side facing up using a gasket and a plastic frame. A 2 g/L dopamine solution in 15 mM TRIS·HCl buffer at pH 8.5 was poured onto the active side of the membrane. The selfpolymerization of dopamine was initiated by placing the membrane onto a rocking platform shaker (60 rpm) while being exposed to oxygen. After a 24 h reaction, the remaining solution on the membrane surface was discarded, and the membrane coupon was rinsed with DI water to remove unbound chemicals and dried under a vacuum. The PDAcoated membrane is denoted as a PES-PDA membrane.

The next step was grafting polymer-SH onto the PES-PDA membrane via Michael addition reaction (Figure S4 and Figure 1b).<sup>35</sup> The PES-PDA membrane was placed on a glass plate, and 40 mL of polymer solution (2 g/L in 15 mM TRIS·HCl buffer, pH 8.5) was poured onto the active side of the membrane. After the membrane was immersed in the solution on the rocking platform shaker (60 rpm) for 24 h, the remaining mixture on the membrane surface was discarded, and the polymer-coated PES-PDA membrane was thoroughly rinsed with DI water and dried under a vacuum. The PNIPAM<sub>68</sub>-, P(NIPAM<sub>34</sub>-r-tEGA<sub>34</sub>)-, P(NIPAM<sub>34</sub>-b-tEGA<sub>34</sub>)-, and P(tEGA<sub>34</sub>-b-NIPAM<sub>34</sub>)-coated PES-PDA membranes are referred to as N-, N-r-T-, N-b-T-, and T-b-N-membrane, respectively.

**Membrane Characterization.** The presence of PDA and thermoresponsive polymer layers was confirmed using X-ray photoelectron spectroscopy (XPS) with a Versa Probe II scanning XPS microprobe (Physical Electronics) using monochromatic Al  $K\alpha$  radiation (1486.6 eV) and ATR-FTIR spectroscopy. Surface morphology of the membranes was characterized by scanning electron microscopy (SEM, SU70, Hitachi) after coating with an 8 nm-thick layer of iridium.

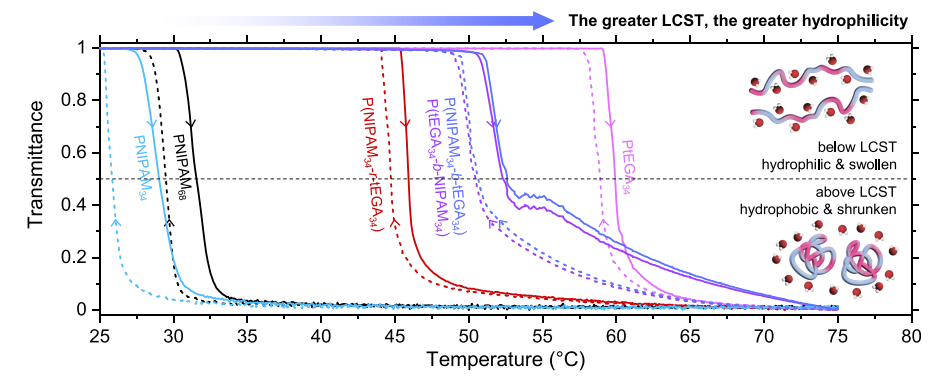


Figure 2. Turbidity measurements by UV—vis spectroscopy at 500 nm. Solid lines correspond to transmittance of a heating curve from 25 to 75 °C at a heating rate of 1 °C min<sup>-1</sup>, while dotted lines correspond to that of a cooling curve from 75 to 25 °C at a colling rate of 1 °C min<sup>-1</sup>.

Atomic force microscopy (AFM, Dimension FastScan, Bruker) in the peak force tapping mode with a silicon tip on silicon nitride cantilever probes (FASTSCAN-B, Bruker) was also used to characterize the morphology and surface roughness of the membranes. The polymer film thickness was determined using ellipsometry (M-2000, J.A. Woollam) at 25 °C to calculate grafting density (see Text S5 for more details). Surface hydrophilicity of the membranes at 25 and 55 °C was determined by measuring water contact angle using the sessile drop method after 10 s.

Water permeability of the pristine and modified membranes was measured with DI water at 25 °C using a dead-end filtration cell (Model 8010, Amicon Corp.) pressurized at 30 psi (~2 bar). The membrane was compacted prior to each test to achieve a stable water flux. Molecular weight cutoff (MWCO) was measured using 0.1 g/L solutions of PEGs with different molecular weights (35, 100, 200, 300, 400, 600, and 4,000 kDa). MWCO was defined as the molecular weight of the PEG that would be rejected 90%. Total organic carbon (TOC) concentration was measured by using a TOC analyzer (TOC-L-CSH, Shimadzu).

Antifouling Evaluation and Fouling Reversibility in Response to Temperature Change Cleaning. In batch adsorption experiments, membrane coupons (2.5 cm²), presoaked in 10 mM PBS, were immersed in 15 mL of 5 g/L BSA solution (10 mM PBS, pH 7.4). After 24 h, adsorbed BSA molecules were detached using 5 wt % SDS for 6 h, and the desorbed BSA concentration was analyzed using UV—vis spectroscopy at 562 nm, based on Micro BCA protein assay kit (ThermoFisher Scientific) standard curve. The same experiment was conducted at two different temperatures; below and above the LCST (25 and 55 °C, respectively).

The dead-end filtration cell was used to perform a dynamic fouling experiment and assess fouling reversibility during temperature-swing cleaning (Figure 1c). The filtration/cleaning process consisted of two cycles, as illustrated in Figure S5a. Each cycle included a 1.5 h precompaction with 10 mM PBS (pH 7.4), a 1.5 h filtration of 1 g/L BSA solution in PBS, and a 20 min backwashing with PBS, resembling typical UF operation systems. The operation and filtration, the operating pressure was set at 30 psi by nitrogen gas, and the temperature was maintained at 25 °C. The initial and final permeate fluxes ( $J_0$  and  $J_{\rm BSA}$ , respectively) were recorded at the beginning and end of the filtration step. Subsequently, the fouled membrane was backwashed with PBS at 55 °C for 20 min. After cooling the membrane coupon to room temperature, the second cycle was performed by repeating the same

procedure. Additionally, another set of experiments was conducted with backwashing at 25 °C. To evaluate fouling resistance of the membrane and the extent of irreversible membrane fouling, total fouling ratio ( $R_{\rm t}$ ), cake layer fouling ratio ( $R_{\rm cake}$ ), removable fouling ratio ( $R_{\rm temp}$ ; removable by temperature-induced conformational change), and irreversible fouling ratio ( $R_{\rm ir}$ ) of the *n*th cycle were calculated by the following equations (Figure S5b):

$$R_{t,n}(\%) = \left(\frac{J_{0,n} - J_{\text{BSA},n}}{J_{0,n}}\right) \times 100\%$$
 (1)

$$R_{\text{cake},n}(\%) = \left(\frac{J_{0,n+1}^* - J_{\text{BSA},n}}{J_{0,n}}\right) \times 100\%$$
 (2)

$$R_{\text{temp},n}(\%) = \left(\frac{J_{0,n+1} - J_{0,n+1}^*}{J_{0,n}}\right) \times 100\%$$
(3)

$$R_{ir,n}(\%) = \left(\frac{J_{0,n} - J_{0,n+1}}{J_{0,n}}\right) \times 100\%$$
(4)

where  $J_{0,n}$  = the initial flux without BSA in the nth cycle,  $J_{\rm BSA,n}$  the final flux after 1.5 h filtration with BSA in nth cycle, and  $J^*_{0,n}$  = the initial flux without BSA in the nth cycle after backwashing at 25 °C. Finally, in order to further investigate the effect of alternate temperature-swing cleaning (Figure 1c), we also conducted the same experiment with a different cleaning process, backwashing at 55 °C for 10 min first and then at 25 °C for 10 min.

## ■ RESULTS AND DISCUSSION

**Polymer Characterization.** The polymerization of both NIPAM and tEGA demonstrated typical characteristics of a living chain-growth process. Pseudo-first-order polymerization kinetics (Figure S3) led to the narrow distribution of molecular weight (D < 1.3) that grew linearly with monomer consumption (Figure S6a and S6b). These observations confirm the successful RAFT polymerization for PNIPAM and PtEGA (see more details in **Text S6**), which are the polymers that will later be grafted onto the membranes. Note that these polymers contain terminal trithiocarbonate functional groups from CTA and hence are termed herein as polymer-CTA.

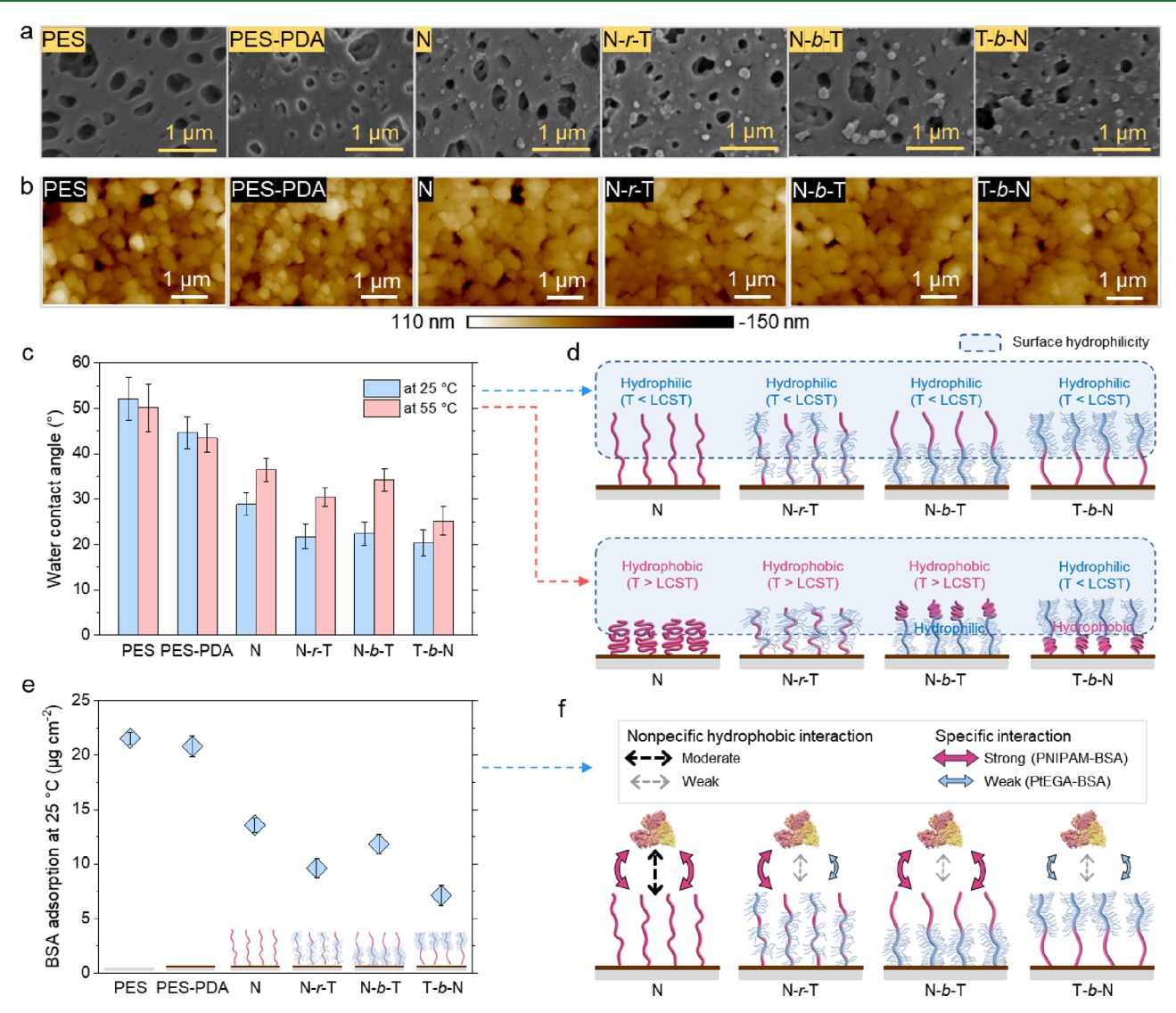


Figure 3. Surface characteristics and static BSA adsorption of the pristine and modified membranes. (a) SEM images of the membranes. (b) 2D AFM images of the membranes. (c) Water contact angle for the membranes at 25 or 55 °C. (d) Schematic diagrams of surface hydrophilicity of the membranes at 25 or 55 °C. Blue boxes with a blue dotted line represent regions affecting surface hydrophilicity measured by water contact angle. (e) BSA adsorption to the membranes at 25 °C. (f) Schematic diagrams of BSA adsorption to the membranes at 25 °C. Black- or gray-dotted arrows represent nonspecific hydrophobic interaction, while red- or blue-filled arrows represent specific interaction between the polymer and BSA. The size of the arrows indicates stronger interactions resulting in higher BSA adsorption. Error bars in panels (c) and (e) represent a standard deviation for five and three different experiments for water contact angle measurement and static adsorption experiment, respectively.

Based on the above kinetics, we deliberately controlled the total DP to be 68 for all the polymers (homo-, random-, and block copolymers), as shown in Figure 1a. In the case of random and block copolymers, the DP was 34 for each PNIPAM and PtEGA block. This control over the DP allowed us to systematically investigate the impact of polymer structure without the complication caused by the effect of DP. We confirmed the DP value of 68 using <sup>1</sup>H NMR spectra (Figure S2) for each polymer by (1) analyzing the ratio between the protons connected to the tertiary carbons in the isopropyl pendant groups of NIPAM units and the methyl protons of the DDMAT chain ends for PNIPAM and (2) analyzing the ratio between the methylene protons of tEGA units and the methyl protons of the DDMAT chain ends for PtEGA. Clear shifts in the GPC traces during the chain extension experiments (Figure S6c) indicated the high end-group fidelity of the trithiocarbonate functional groups in the first blocks (PNIPAM<sub>34</sub>-CTA

and PtEGA<sub>34</sub>–CTA), ensuring the successful synthesis of block copolymers.<sup>37</sup> Moreover, the microphase separation observed in the SAXS profiles (Figure S6d) confirmed the block arrangement of monomeric units in the block copolymers. In contrast, the SAXS profile of the random polymer did not show a microphase separation of the PtEGA groups.

**LCST Evaluation.** Next, we evaluated the temperature responsiveness and changes in the hydrophilicity of the polymer–CTAs (Figure 2). The homopolymer PNIPAM $_{68}$ –CTA exhibited an LCST of 30.6 °C, which closely aligns with the widely reported LCST of approximately 32 °C for atactic PNIPAM. We further synthesized a shorter PNIPAM with DP of 34, PNIPAM $_{34}$ –CTA, which is the first block of P(NIPAM $_{34}$ -b-tEGA $_{34}$ )–CTA. The shorter PNIPAM $_{34}$  chain showed a slightly lower LCST of 27.4 °C compared to the longer PNIPAM $_{68}$  chain, likely due to the hydrophobic alkyl

chain  $(-C_{12}H_{25})$  in DDMAT (used as CTA during the synthesis) exerting a greater influence on the shorter PNIPAM chain's interaction with water.<sup>38,39</sup> PtEGA<sub>34</sub>–CTA, the first block of P(tEGA<sub>34</sub>-b-NIPAM<sub>34</sub>)–CTA, had an LCST of around 59.4 °C, consistent with the previous literature,<sup>40</sup> which further confirmed the higher hydrophilicity of PtEGA compared to PNIPAM.

The random copolymer exhibited average characteristics of both PNIPAM and PtEGA, with an LCST of 45.3 °C which is approximately the average of the LCST values of the two homopolymers. Additionally, the random copolymer displayed a sharp change in transmittance around its LCST, similar to the case for the homopolymers. In contrast, the block copolymers exhibited two-stage transitions for the individual blocks: a sharp transmittance drop around 52 °C and a gradual change from 55.5 to 70 °C, corresponding to the conformational change of the PNIPAM and PtEGA blocks, respectively. This was more pronounced in the heating curve, which showed a plateau at 53–55 °C. The observation of two separate LCSTs in the diblock copolymers is consistent with previous studies, and it is known that the LCST of each block is affected by the lengths and hydrophilicity/hydrophobicity of the neighboring blocks.31

It is noteworthy that the LCST of the PNIPAM block in the block copolymer was significantly higher than that of the PNIPAM homopolymer, since the neighboring hydrophilic PtEGA block with the same DP can retard the build-up or breakdown of the hydrogen bonding required for the conformational change of PNIPAM. 41 The PtEGA block in the block copolymers exhibited a hydrophilic-to-hydrophobic transition starting at 55.5 °C during heating, which was lower than the LCST of the PtEGA homopolymer. This can be attributed to the hydrophobic PNIPAM block interrupting hydrogen bonding. The cooling curve did not exhibit a plateau but two distinct stages corresponding to the PNIPAM and PtEGA blocks. Hysteresis in the cooling curve has also been reported in other studies, due to the formation of additional inter- and intrachain hydrogen bonds in the collapsed state.<sup>31</sup> Based on Figure 2 and Text S7, we determined a water temperature of 55 °C as the optimal temperature for inducing the thermal conformation transition during membrane cleaning. This temperature surpasses the LCST values of the PNIPAM homopolymer, the random copolymer, and the PNIPAM block in the block copolymers. Also, it remains sufficiently low to prevent the hydrophilic-to-hydrophobic transition of the PtEGA block in the block copolymers.

Chain-End Transformation to Thiols. We further modified the polymer-CTAs by converting their trithiocarbonate terminal groups to thiol groups via aminolysis (Figure 1a). The loss of the trithiocarbonate group was confirmed by UV-vis absorption at 310 nm (Figure S7a). The structure of the resulting polymer-SHs was also evaluated by <sup>1</sup>H NMR spectroscopy in Figure S7b, which exhibited a significant reduction in peak intensity for the protons in the methyl group of the trithiocarbonate chain end after aminolysis. Finally, FTIR spectra in Figure S7c confirmed the presence of characteristic bands associated with thioester, dithioester, and thiocarbonyl groups (610, 750, 1050, 1082, and 1255 cm<sup>-1</sup>)<sup>42,43</sup> in PNIPAM<sub>68</sub>-CTA but not in PNIPAM<sub>68</sub>-SH. Afterward, these polymer-SHs were grafted onto the membranes following the procedure described in the Experimental section.

Morphological characterization of modified membranes. We confirmed the successful PDA layer coating and subsequent polymer grafting onto the membrane surface via XPS analysis (Figure S8 and Table S1) and the FTIR spectrum (Figure S9), as described in more detail in Text S8. We also confirmed that grafting densities among the polymer-grafted membranes remained constant. Grafting density is one of the most critical factors affecting surface and membrane properties, adsorption behavior, and temperature-induced changes in polymer conformation. 44,45 The grafting density was calculated using the equation  $\sigma = (N_{\rm A}h\rho)/(M_{\rm n})$ , where  $N_{\rm A}$  is Avogadro's number, h is the film thickness, and  $\rho$  is the density of the dry polymer. The film thicknesses of the four different polymers at 25 °C were determined by using an ellipsometer (Text S5 and Table S2). The PNIPAM homopolymer layer exhibited a film thickness of 2.3 nm, which is consistent with a previous study reporting a thickness of 2.7 nm for short PNIPAM brushes  $(M_n \sim 12 \text{ kDa})$  on gold substrates prepared via a grafting-to approach. 46 All copolymer films displayed a comparable film thickness (~2.9 nm) with no significant differences. Estimated grafting densities are summarized in Table S2 (refer to Text S9 for detailed calculations).

The surface morphologies of the pristine and modified membranes were also mostly consistent, as assessed based on SEM (Figure 3a), AFM (Figure 3b and S11), and the rootmean-square roughness  $(R_q)$  values analysis (Table S2). The pristine PES membrane displayed a smooth surface with an  $R_q$ of 34.4 nm and pores at  $\sim 0.1 \mu m$ . Although we observed a color change of the membrane to brown after PDA coating, the SEM and AFM images indicated no substantial alteration in the microscopic morphology. The  $R_q$  value slightly decreased to 25.8 nm, indicating that PDA was uniformly coated on the surface. Likewise, the polymer films had a negligible impact on the surface morphology of the membrane (Figure 3a,b), and there was no statistically significant difference in the surface roughness between the PES-PDA and polymer-coated membranes. Results so far enabled us to rule out the impact of grafting density and morphological differences on membrane performance variation. Consistently, water permeability under the same pressure and MWCO at 25 °C remained relatively constant (Table S2 and Figure S12).

Surface Hydrophilicity and Static Protein Adsorption. Despite inducing minimal changes in water permeability and solute rejection, the polymer coating significantly increased surface hydrophilicity. The surface hydrophilicity of the membranes was first evaluated at 25 °C by measuring the water contact angles (Figure 3c). The PES membrane exhibited moderate hydrophilicity, with a contact angle of 52.1° at 25 °C. After PDA coating, the contact angle decreased slightly to 44.6° due to the hydrophilic moieties in PDA. The contact angle further decreased after polymer grafting, indicating an increase in the surface hydrophilicity. As we have intended, the copolymer grafted-membranes (N-r-T-, Nb-T-, and T-b-N-membranes) exhibited higher hydrophilicity with a contact angle of 20.5–22.4° compared to the N-membrane with the contact angle of 28.9°. 47,48

When the temperature was increased to 55 °C, the hydrophilicity of the PES and PES-PDA membranes, which lack temperature-responsive moieties, remained unchanged. In contrast, all the polymer-grafted membranes displayed a reduction in hydrophilicity (average 36% increase in contact angle) as the temperature increased to 55 °C, consistent with past studies that have reported changes in water contact angle

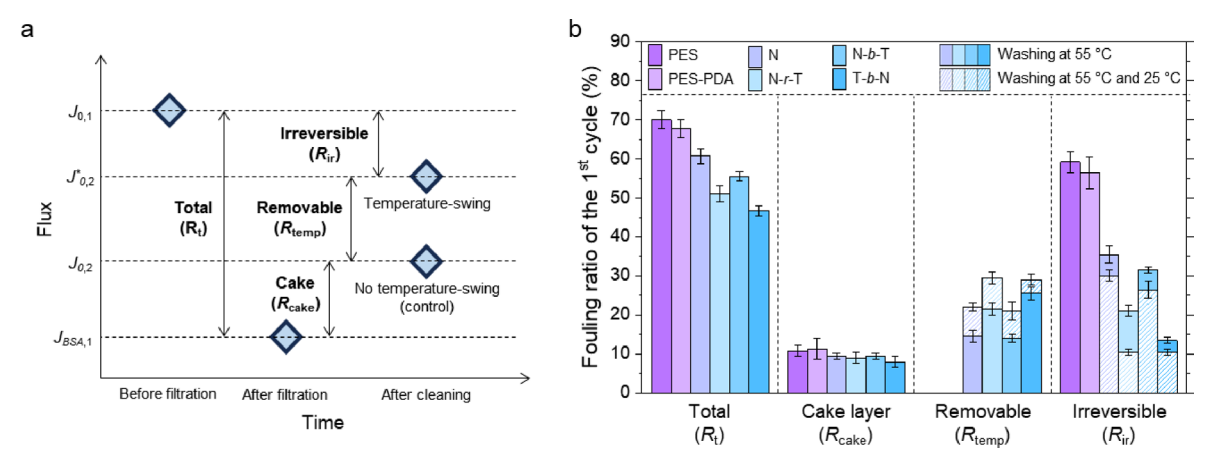


Figure 4. Antifouling and fouling reversibility of the pristine and modified membranes. (a) Schematic illustration of dynamic fouling experiment and the calculation of fouling ratios (see Figure S5 for more details). (b) Fouling ratio of the 1st cycle of dynamic protein fouling experiment. Total fouling ( $R_{\rm t}$ ), cake layer fouling ( $R_{\rm cake}$ ), removable fouling by a temperature-induced conformational change ( $R_{\rm temp}$ ), and irreversible fouling ( $R_{\rm temp}$ ) were calculated from eqs 1–4. For  $R_{\rm temp}$  and  $R_{\rm ir}$ , the solid bars denote results from the single-temperature-swing cleaning process, while the shaded bars correspond to outcomes from the alternate temperature-swing cleaning process. Error bars represent a standard deviation for two different experiments.

on thermoresponsive polymer-grafted surfaces across the LCST. <sup>49,50</sup> We observed that the surface hydrophilicity at 55 °C followed the order of N-, N-*b*-T-, N-*r*-T-, and T-*b*-N-membrane. (Figure 3c and 3d).

The increase in surface hydrophilicity led to a reduction in the interaction of the membrane surface with BSA at 25 °C (Figure 3e). A control experiment confirmed that the change in BSA adsorption was not due to the addition of PDA layer. BSA adsorption followed a decreasing trend in the order of N-, N-b-T-, N-r-T-, and T-b-N-membrane, which correlates with the order of decreasing surface hydrophilicity. <sup>19,51,52</sup> A similar trend was observed in BSA adsorption at 55 °C (Text S10 and Figure S13). These observations confirm that enhancing surface hydrophilicity through polymer grafting effectively mitigates nonspecific interactions between the membrane and BSA at temperatures below the LCST. <sup>53,54</sup>

It is noteworthy that although all the copolymer-grafted membranes contain the same amount and type of functional groups (i.e., identical DP of PNIPAM and PtEGA), the T-b-Nmembrane demonstrated the highest hydrophilicity and the lowest BSA adsorption. The T-b-N-membrane also exhibited the least change in hydrophilicity with a temperature change. Previous studies have demonstrated that surfaces containing hydrogen-bond donors more strongly adsorb BSA due to the formation of strong hydrogen bonds between the surface and BSA, 19,51,55,56 which is the case for the N-membrane. On the other hand, surfaces incorporating ethylene-glycol derivates such as PEG generally exhibit high resistance to BSA adsorption due to their hydrophilicity and steric effects. 55,57,58 We estimate that the distance between grafting sites, based on the grafting density, would be approximately 2.4 nm (Text S9 and Table S2). These gaps are smaller than the hydrodynamic diameter of BSA molecules at ambient temperature (~7 nm).<sup>48,59</sup> Therefore, it is unlikely that BSA molecules penetrate the interspace between polymer brushes. Instead, in the case of T-b-N-membrane, the hydrophilic PtEGA block of the T-b-Nmembrane would shield the hydrophobic PNIPAM block that lies underneath from interacting with BSA,<sup>22</sup> thereby reducing overall BSA adsorption. Based on these findings, we conclude that the arrangement of monomers in copolymers plays a crucial role in determining the surface properties of polymercoated membranes (Figure 3f). Specifically, the identity of the functional groups facing outward and in contact with water is critical in influencing the surface hydrophilicity and protein adsorption behavior. <sup>19,51,58</sup>

Surface cleaning performance via temperature change cleaning cycles. We then examined how the aforementioned changes in surface hydrophilicity and BSA adsorption affect the antifouling property and fouling reversibility. The  $R_{tr}$   $R_{cake}$ ,  $R_{temp}$ , and  $R_{ir}$  values (Figure 4a and Figure S5) for the dynamic fouling experiments are shown in Figure 4b. The R<sub>t</sub> value represents the flux decrease due to both reversible and irreversible fouling. We observed that the pristine PES membrane exhibited the highest  $R_t$  value of 70% (i.e., a 70% flux decline). The addition of the PDA layer did not significantly affect the R<sub>t</sub> value for the PES-PDA membrane. In contrast, the polymer films resulted in a noticeable decrease in the R<sub>t</sub> value for the polymer-grafted membranes. The R<sub>t</sub> values decreased in the following order: N-, N-b-T-, N-r-T-, and T-b-N-membrane, once again consistent with the tendency for increasing surface hydrophilicity and decreasing BSA adsorption at  $25~^{\circ}\text{C}$  (Figure 3c).

A closer examination of the fouling mechanism ( $R_{\text{cake}}$ ,  $R_{\text{temp}}$ , and  $R_{ir}$ ) suggests that  $R_{cake}$  (flux reduction by the formation of a cake layer) remained relatively constant across all of the membranes at approximately 10%. In stark contrast, both  $R_{\text{temp}}$ (the extent of flux recovery during temperature-swing cleaning) and Rir (the fraction of flux that remains irrecoverable after the filtration-cleaning cycle) varied significantly depending on the polymer coating. In the case of the PES and PES-PDA membranes, which do not contain thermoresponsive polymers, there were negligible differences in flux recovery between backwashing at 55 and 25 °C, resulting in  $R_{\text{temp}}$  being zero. Consequently, the average  $R_{\text{ir}}$ value for the PES and PES-PDA membranes was substantial at 58%, contributing to nearly 85% of the total fouling and leading to a significant decline in the flux in subsequent filtration cycles.

We observed that grafting thermoresponsive polymers onto the membranes not only decreased irreversible fouling ( $R_{\rm ir}$ decreased in the order of N-, N-b-T-, N-r-T-, and T-b-Nmembranes (36%, 32%, 21%, and 14%, respectively) but also significantly improved flux recovery during elevated temperature backwashing at 55 °C ( $R_{\text{temp}} > 0$ ). We also observed that the order of  $R_{\text{temp}}$  (N-  $\approx$  N-b-T- < N-r-T- < and T-b-Nmembrane) aligned with the surface hydrophilicity at 55 °C (Figure 3c). While the temperature-induced conformational change and disruption of interactions between the surface and BSA contributed to flux recovery in all these modified membranes, 14,22,60 the higher surface hydrophilicity appeared beneficial for enhancing temperature-induced BSA desorption and reducing irreversible fouling at 55 °C.<sup>22</sup> In the second cycle, we consistently observed a similar trend in fouling ratios (Figure S14a), with the T-b-N-membrane exhibiting the lowest values of  $R_t$  (45%) and  $R_{ir}$  (17%). Considering the median backwash interval of 30 min for ultrafiltration membranes under pressure mode, 61 the T-b-N-membranes demonstrated the greatest fouling reversibility in several cycles of 1.5 h dynamic protein fouling tests (Figure S14b).

Finally, we examined the effect of the alternate temperature-swing backwashing scheme <sup>14,22,60,62</sup> on the fouling reversibility using a different cleaning process that involved an initial backwashing at 55 °C followed by a subsequent backwashing at 25 °C (Figure 1c and Figure S15). We observed no change in  $R_{ir}$  for the PES and PES-PDA membranes when compared to the single-step backwashing at 55 °C. However, all of the polymer-grafted membranes exhibited a meaningful increase in  $R_{\text{temp}}$  with the additional lower-temperature backwashing. This is likely because the thermoresponsive polymer underwent an additional conformational change, transitioning from a shrunken to a swelling state and regaining its hydrophilic nature when the backwashing temperature was switched from 55 to 25 °C. This additional disturbance facilitated the detachment of foulants that were not previously removed during backwashing at 55 °C.60 These findings underscore the potential of alternative temperature change cleaning to further improve fouling reversibility in combination with tailored monomer arrangements.

### **■ ENVIRONMENTAL IMPLICATIONS**

By grafting well-defined thermoresponsive polymers onto the membrane while controlling the DP and grafting density, we have successfully unraveled for the first time the significance of monomer arrangements on both the fouling resistance and reversibility. A strategy to place a hydrophilic polymer block on top of the thermoresponsive polymer enhances the surface hydrophilicity and antifouling properties, while maintaining thermoresponsive capability that is essential for the temperature-swing cleaning scheme. We argue that these findings are important in designing small-scale membrane-based water treatment units that can be employed in LMICs, where using warm water instead of other chemical-based cleaning is expected to be particularly useful. We recognize that the polymer structure investigated in this study, namely, random and block copolymerization, is one representative example among many possible polymer architecture options. By leveraging advanced polymerization techniques and characterization tools, we anticipate that further research is needed to discover copolymer designs with optimal chemical identity and DP for effective surface fouling control based on simple temperature-swing schemes. Also, a comprehensive evaluation of the cleaning temperature, taking into account both cleaning efficiency and operational costs, should be conducted to ensure the practical applicability of our findings.

#### ASSOCIATED CONTENT

# Supporting Information

The Supporting Information is available free of charge at https://pubs.acs.org/doi/10.1021/acs.est.3c05514.

(i) Details of polymer synthesis and characterization including <sup>1</sup>H NMR spectra, GPC traces, UV—vis spectra, FTIR spectra, and SAXS profiles of the polymers, (ii) description of ellipsometry experiment and calculation of grafting density and distance between grafting sites, (iii) LCST behavior at the rapid temperature-change cleaning process, (iv) surface characterization of the pristine and modified membranes including XPS spectra, FTIR spectra, and 3D AFM images, (v) water permeability and MWCO of the membranes, (vi) schematic illustration of dynamic fouling experiment, and (vii) BSA adsorption at 55 °C and fouling ratio and normalized water flux over multiple cycles (PDF)

#### AUTHOR INFORMATION

#### **Corresponding Authors**

Jae-Hong Kim — Department of Chemical and Environmental Engineering, Yale University, New Haven, Connecticut 06511, United States; orcid.org/0000-0003-2224-3516; Phone: +1 (203) 432-4386; Email: jaehong.kim@yale.edu Mingjiang Zhong — Department of Chemical and Environmental Engineering, Yale University, New Haven, Connecticut 06511, United States; orcid.org/0000-0001-7533-4708; Phone: +1 (203) 432-5790; Email: mingjiang.zhong@yale.edu

# Authors

Inhyeong Jeon — Department of Chemical and Environmental Engineering, Yale University, New Haven, Connecticut 06511, United States; ⊚ orcid.org/0000-0002-0341-4626

Junwoo Lee — Department of Chemical and Environmental Engineering, Yale University, New Haven, Connecticut 06511, United States

Complete contact information is available at: https://pubs.acs.org/10.1021/acs.est.3c05514

#### **Author Contributions**

<sup>#</sup>I.J. and J.L. contributed equally.

#### Notes

The authors declare no competing financial interest.

#### ACKNOWLEDGMENTS

I.J. was partly supported by the Kwanjeong Fellowship from the Kwanjeong Educational Foundation. J.L. was supported by Basic Science Research Program through the National Research Foundation of Korea (NRF) funded by the Ministry of Education (2021R1A6A3A14038599). This work was also partly supported by National Science Foundation (CHE-1845184).

# **■** REFERENCES

- (1) United Nations Children's Fund; World Health Organization *Progress on household drinking water, sanitation and hygiene* 2000–2017; Special focus on inequalities: New York, USA, 2019.
- (2) United Nations The Millennium Development Goals Report 2015; United Nations: New York, NY, 2015.
- (3) UN WaterSustainable Development Goal 6: Synthesis Report 2018 on Water and Sanitation; United Nations: New York, NY, 2018.

- (4) Arnal, J. M.; Garcia-Fayos, B.; Verdu, G.; Lora, J. Ultrafiltration as an alternative membrane technology to obtain safe drinking water from surface water: 10 years of experience on the scope of the AOUAPOT project. *Desalination* **2009**, *248*, 34–41.
- (5) Zhang, X.; He, Y.; Zhang, B.; Qin, L.; Yang, Q.; Huang, H. Factors affecting microbiological quality of household drinking water supplied by small-scale ultrafiltration systems: A field study. *Sci. Total Environ.* **2019**, *689*, 725–733.
- (6) Elimelech, M.; Phillip, W. A. The future of seawater desalination: energy, technology, and the environment. *Science* **2011**, 333, 712–717.
- (7) Mauter, M. S.; Zucker, I.; Perreault, F.; Werber, J. R.; Kim, J.-H.; Elimelech, M. The role of nanotechnology in tackling global water challenges. *Nat. Sustain.* **2018**, *1*, 166–175.
- (8) Jim, K. J.; Fane, A. G.; Fell, C. J. D.; Joy, D. C. Fouling mechanisms of membranes during protein ultrafiltration. *J. Membr. Sci.* 1992, 68, 79–91.
- (9) Rana, D.; Matsuura, T. Surface modifications for antifouling membranes. *Chem. Rev.* **2010**, *110* (4), 2448–2471.
- (10) Subasi, Y.; Cicek, B. Recent advances in hydrophilic modification of PVDF ultrafiltration membranes—a review: part I. *Membr. Technol.* **2017**, 2017, 7–12.
- (11) Boerlage, Ś. F. E.; Kennedy, M. D.; Aniye, M. P.; Abogrean, E. M.; El-Hodali, D. E. Y.; Tarawneh, Z. S.; Schippers, J. C. Modified Fouling Indexultrafiltration to compare pretreatment processes of reverse osmosis feedwater. *Desalination* **2000**, *131*, 201–214.
- (12) Liu, Z.; Wang, W.; Xie, R.; Ju, X. J.; Chu, L. Y. Stimuli-responsive smart gating membranes. *Chem. Soc. Rev.* **2016**, *45*, 460–475.
- (13) Kwon, O. H.; Kikuchi, A.; Yamato, M.; Okano, T. Accelerated cell sheet recovery by co-grafting of PEG with PIPAAm onto porous cell culture membranes. *Biomaterials* **2003**, *24*, 1223–1232.
- (14) Guo, H.; Huang, J.; Wang, X. The alternate temperature-change cleaning behaviors of PNIPAAm grafted porous polyethylene membrane fouled by proteins. *Desalination* **2008**, 234, 42–50.
- (15) Cho, E. C.; Kim, Y. D.; Cho, K. Temperature-dependent intermolecular force measurement of poly (N-isopropylacrylamide) grafted surface with protein. *J. Colloid Interface Sci.* **2005**, 286, 479–486.
- (16) Heskins, M.; Guillet, J. E. Solution properties of poly (N-isopropylacrylamide). *J. Macromol. Sci. A* **1968**, *2*, 1441–1455.
- (17) Schild, H. G. Poly (N-isopropylacrylamide): experiment, theory and application. *Prog. Polym. Sci.* **1992**, *17*, 163–249.
- (18) Adout, A.; Kang, S.; Asatekin, A.; Mayes, A. M.; Elimelech, M. Ultrafiltration membranes incorporating amphiphilic comb copolymer additives prevent irreversible adhesion of bacteria. *Environ. Sci. Technol.* **2010**, *44*, 2406–2411.
- (19) Ostuni, E.; Chapman, R. G.; Holmlin, R. E.; Takayama, S.; Whitesides, G. M. A survey of structure—property relationships of surfaces that resist the adsorption of protein. *Langmuir* **2001**, *17*, 5605–5620
- (20) Wandera, D.; Himstedt, H. H.; Marroquin, M.; Wickramasinghe, S. R.; Husson, S. M. Modification of ultrafiltration membranes with block copolymer nanolayers for produced water treatment: the roles of polymer chain density and polymerization time on performance. *J. Membr. Sci.* **2012**, *403*, 250–260.
- (21) Wandera, D.; Wickramasinghe, S. R.; Husson, S. M. Modification and characterization of ultrafiltration membranes for treatment of produced water. *J. Membr. Sci.* **2011**, *373*, 178–188.
- (22) Ye, Y.; Huang, J.; Wang, X. Fabrication of a self-cleaning surface via the thermosensitive copolymer brush of P (NIPAAm-PEGMA). ACS Appl. Mater. Interfaces 2015, 7, 22128–22136.
- (23) Bittrich, E.; Burkert, S.; Müller, M.; Eichhorn, K. J.; Stamm, M.; Uhlmann, P. Temperature-sensitive swelling of poly (N-isopropylacrylamide) brushes with low molecular weight and grafting density. *Langmuir* **2012**, 28, 3439–3448.
- (24) Yim, H.; Kent, M. S.; Mendez, S.; Lopez, G. P.; Satija, S.; Seo, Y. Effects of grafting density and molecular weight on the temperature-dependent conformational change of poly (N-isopropy-

- lacrylamide) grafted chains in water. *Macromolecules* **2006**, 39, 3420–3426.
- (25) Zhang, Y.; Panneerselvam, K.; Ogaki, R.; Hosta-Rigau, L.; Van Der Westen, R.; Jensen, B. E.; Teo, B. M.; Zhu, M.; Städler, B. Assembly of poly (dopamine)/poly (N-isopropylacrylamide) mixed films and their temperature-dependent interaction with proteins, liposomes, and cells. *Langmuir* 2013, 29, 10213–10222.
- (26) Biggs, C. I.; Walker, M.; Gibson, M. I. Grafting to" of RAFTed responsive polymers to glass substrates by thiol—ene and critical comparison to thiol—gold coupling. *Biomacromolecules* **2016**, *17*, 2626–2633.
- (27) Zoppe, J. O.; Ataman, N. C.; Mocny, P.; Wang, J.; Moraes, J.; Klok, H.-A. Surface-initiated controlled radical polymerization: state-of-the-art, opportunities, and challenges in surface and interface engineering with polymer brushes. *Chem. Rev.* **2017**, *117*, 1105–1318.
- (28) Schweigerdt, A.; Heinen, S.; Stöbener, D. D.; Weinhart, M. Grafting density-dependent phase transition mechanism of thermoresponsive poly (glycidyl ether) brushes: A comprehensive QCM-D study. *Langmuir* **2021**, *37*, 7087–7096.
- (29) Perrier, S. 50th Anniversary Perspective: RAFT Polymerization— A User Guide. *Macromolecules* **2017**, 50, 7433–7447.
- (30) Yamauchi, H.; Maeda, Y. LCST and UCST behavior of poly (N-isopropylacrylamide) in DMSO/water mixed solvents studied by IR and micro-Raman spectroscopy. *J. Phys. Chem. B* **2007**, *111*, 12964–12968.
- (31) Strandman, S.; Zhu, X. X. Thermo-responsive block copolymers with multiple phase transition temperatures in aqueous solutions. *Prog. Polym. Sci.* **2015**, 42, 154–176.
- (32) Willcock, H.; O'Reilly, R. K. End group removal and modification of RAFT polymers. *Polym. Chem.* **2010**, *1*, 149–157.
- (33) McCloskey, B. D.; Park, H. B.; Ju, H.; Rowe, B. W.; Miller, D. J.; Chun, B. J.; Kin, K.; Freeman, B. D. Influence of polydopamine deposition conditions on pure water flux and foulant adhesion resistance of reverse osmosis, ultrafiltration, and microfiltration membranes. *Polymer* **2010**, *51*, 3472–3485.
- (34) Lee, H.; Dellatore, S. M.; Miller, W. M.; Messersmith, P. B. Mussel-inspired surface chemistry for multifunctional coatings. *Science* **2007**, *318*, 426–430.
- (35) Shahkaramipour, N.; Lai, C. K.; Venna, S. R.; Sun, H.; Cheng, C.; Lin, H. Membrane surface modification using thiol-containing zwitterionic polymers via bioadhesive polydopamine. *Ind. Eng. Chem. Res.* **2018**, *57*, 2336–2345.
- (36) Abdul Azis, P. K.; Al-Tisan, I.; Sasikumar, N. Biofouling potential and environmental factors of seawater at a desalination plant intake. *Desalination* **2001**, *135*, 69–82.
- (37) Keddie, D. J. A guide to the synthesis of block copolymers using reversible-addition fragmentation chain transfer (RAFT) polymerization. *Chem. Soc. Rev.* **2014**, *43*, 496–505.
- (38) Halperin, A.; Kröger, M.; Winnik, F. M. Poly (N-isopropylacrylamide) phase diagrams: fifty years of research. *Angew. Chem., Int. Ed.* **2015**, 54, 15342–15367.
- (39) Furyk, S.; Zhang, Y.; Ortiz-Acosta, D.; Cremer, P. S.; Bergbreiter, D. E. Effects of end group polarity and molecular weight on the lower critical solution temperature of poly (N-isopropylacrylamide). *J. Polym. Sci. A Polym. Chem.* **2006**, 44, 1492–1501.
- (40) Badi, N. Non-linear PEG-based thermoresponsive polymer systems. *Prog. Polym. Sci.* **2017**, *66*, 54–79.
- (41) Mäkinen, L.; Varadharajan, D.; Tenhu, H.; Hietala, S. Triple hydrophilic UCST-LCST block copolymers. *Macromolecules* **2016**, 49, 986–993.
- (42) Rao, C. N. R.; Venkataraghavan, R. The C= S stretching frequency and the "- N- C= S bands" in the infrared. *Spectrochim. Acta A Mol. Biomol. Spectrosc.* **1989**, 45, 299–305.
- (43) Wiles, D. M.; Gingras, B. A.; Suprunchuk, T. The C= S stretching vibration in the infrared spectra of some thiosemicarbazones. *Can. J. Chem.* **1967**, *45*, 469–473.
- (44) Choi, B. C.; Choi, S.; Leckband, D. E. Poly (N-isopropyl acrylamide) brush topography: dependence on grafting conditions and temperature. *Langmuir* **2013**, *29*, 5841–5850.

- (45) Xue, C.; Yonet-Tanyeri, N.; Brouette, N.; Sferrazza, M.; Braun, P. V.; Leckband, D. E. Protein adsorption on poly (N-isopropylacrylamide) brushes: dependence on grafting density and chain collapse. *Langmuir* **2011**, *27*, 8810–8818.
- (46) Zhang, G. Study on conformation change of thermally sensitive linear grafted poly (N-isopropylacrylamide) chains by quartz crystal microbalance. *Macromolecules* **2004**, *37*, 6553–6557.
- (47) Maas, J. H.; Fleer, G. J.; Leermakers, F. A. M.; Cohen Stuart, M. A. Wetting of a polymer brush by a chemically identical polymer melt: Phase diagram and film stability. *Langmuir* **2002**, *18*, 8871–8880.
- (48) Brittain, W. J.; Minko, S. A structural definition of polymer brushes. J. Polym. Sci. A Polym. Chem. 2007, 45, 3505-3512.
- (49) Zhuang, P.; Dirani, A.; Glinel, K.; Jonas, A. M. Temperature dependence of the surface and volume hydrophilicity of hydrophilic polymer brushes. *Langmuir* **2016**, *32*, 3433–3444.
- (50) Yu, J. Z.; Zhu, L. P.; Zhu, B. K.; Xu, Y. Y. Poly (N-isopropylacrylamide) grafted poly (vinylidene fluoride) copolymers for temperature-sensitive membranes. *J. Membr. Sci.* **2011**, *366*, 176–183.
- (51) Contreras, A. E.; Steiner, Z.; Miao, J.; Kasher, R.; Li, Q. Studying the role of common membrane surface functionalities on adsorption and cleaning of organic foulants using QCM-D. *Environ. Sci. Technol.* **2011**, *45*, 6309–6315.
- (52) Sigal, G. B.; Mrksich, M.; Whitesides, G. M. Effect of surface wettability on the adsorption of proteins and detergents. *J. Am. Chem. Soc.* **1998**, *120*, 3464–3473.
- (53) Möckel, D.; Staude, E.; Guiver, M. D. Static protein adsorption, ultrafiltration behavior and cleanability of hydrophilized polysulfone membranes. *J. Membr. Sci.* **1999**, *158*, 63–75.
- (54) Li, L.; Yin, Z.; Li, F.; Xiang, T.; Chen, Y.; Zhao, C. Preparation and characterization of poly (acrylonitrile-acrylic acid-N-vinyl pyrrolidinone) terpolymer blended polyethersulfone membranes. *J. Membr. Sci.* **2010**, 349, 56–64.
- (55) Herrwerth, S.; Eck, W.; Reinhardt, S.; Grunze, M. Factors that determine the protein resistance of oligoether self-assembled monolayers— internal hydrophilicity, terminal hydrophilicity, and lateral packing density. *J. Am. Chem. Soc.* **2003**, *125*, 9359–9366.
- (56) Chapman, R. G.; Ostuni, E.; Takayama, S.; Holmlin, R. E.; Yan, L.; Whitesides, G. M. Surveying for surfaces that resist the adsorption of proteins. *J. Am. Chem. Soc.* **2000**, *122*, 8303–8304.
- (57) Roach, P.; Farrar, D.; Perry, C. C. Interpretation of protein adsorption: surface-induced conformational changes. *J. Am. Chem. Soc.* **2005**, *127*, 8168–8173.
- (58) Sethuraman, A.; Han, M.; Kane, R. S.; Belfort, G. Effect of surface wettability on the adhesion of proteins. *Langmuir* **2004**, *20*, 7779–7788.
- (59) Dai, W.; Zheng, C.; Zhao, B.; Chen, K.; Jia, P.; Yang, J.; Zhao, J. A negative correlation between water content and protein adsorption on polymer brushes. *J. Mater. Chem. B* **2019**, *7*, 2162–2168.
- (60) Zhou, S.; Xue, A.; Zhang, Y.; Li, M.; Wang, J.; Zhao, Y.; Xing, W. Fabrication of temperature-responsive ZrO2 tubular membranes, grafted with poly (N-isopropylacrylamide) brush chains, for protein removal and easy cleaning. *J. Membr. Sci.* **2014**, *450*, 351–361.
- (61) Chang, H.; Zhu, Y.; Yu, H.; Qu, F.; Zhou, Z.; Li, X.; Yang, Y.; Tang, X.; Liang, H. Long-term operation of ultrafiltration membrane in full-scale drinking water treatment plants in China: Characteristics of membrane performance. *Desalination* **2022**, 543, No. 116122.
- (62) Cross, M. C.; Toomey, R. G.; Gallant, N. D. Protein-surface interactions on stimuli-responsive polymeric biomaterials. *Biomed Mater.* **2016**, *11*, No. 022002.